The Injection of Solids Using a Reactive Carrier Gas

D.E. LANGBERG and M. NILMANI

The injection of nonwettable powders into melts in the bubbling regime was studied experimentally using a cold-model system. Polyethylene powder was injected into a cylindrical vessel containing water, through a vertical top-submerged lance, with insoluble (air) and soluble (ammonia) carrier gases. The concentration of particles in the liquid and the penetration length of the particle-liquid jet into the bath were measured, as the carrier gas composition, the gas and solids flow rates, and the particle size were varied. It was found that the concentration of particles retained in the liquid was up to 10 times higher, and the penetration length of the jet was up to three times higher when the soluble carrier gas was used instead of the insoluble carrier gas. For both carrier gases, the dispersed particle concentration increased with increasing gas flow rate and increasing particle size, whereas the penetration length of the jet increased with increasing gas and solids flow rates.

I. INTRODUCTION

EFFECTIVE injection of powders into melts requires the efficient disengagement of the particles from the carrier gas in order to become exposed to the melt and sufficient residence time for them to react or dissolve before surfacing or sedimenting. The disengagement of coarse particles injected at low solids loadings, which occurs by penetration through a bubble-liquid interface, has been the subject of several studies.[1,2,3] It is generally concluded that large, dense, wettable particles are relatively easy to inject, but poor injection efficiencies are encountered when injecting fine, low density, nonwettable particles. When fine particles are injected at high solids loadings, coupling between the phases results in gas-solid jet formation at the lance tip.[4,5,6] Disengagement between the particles and the gas when the jet disintegrates is not well understood. It is likely that many particles remain attached to the bubbles due to the low relative velocity between the solid and gas phases in the coupled flow.[7]

The residence time of the particles is determined by their velocity relative to the melt and by the bulk flow velocity of the melt. If the particles have low settling velocities, their motion will be controlled by the bulk circulation generated by the bubble plume. If they remain in the vicinity of the lance tip upon injection, they will be rapidly carried by the plume to the upper surface of the melt with a low utilization efficiency.

In many systems of practical interest such as lime injection with oxygen as the carrier gas into steel[8] and flux injection with air through tuyeres into a Pierce-Smith converter,[9] the carrier gases strongly react with the melt. In some important systems (Fe-O, Cu-O), the presence of a reactive gas can reduce the surface tension of the gas-melt interface[10,11] and, hence, lower the interfacial resistance to particle penetration of the bubble surface. Furthermore, the elimination of the bubble plume by the dissolution of the carrier gas will significantly reduce the bulk flow velocity of the melt[12,13] and potentially increase the residence time of the injected particles.

This article addresses experimentally the differences in the hydrodynamic behavior that occur when a soluble rather than an insoluble carrier gas is used for solids injection. A cold-model analog system was used in which polyethylene particles were injected into a cylindrical vessel containing water, through a top-submerged vertical lance. The carrier gases used were air (insoluble) and ammonia (soluble). The degree of dispersion of the injected particles and the penetration distance of the particles into the liquid were measured as the gas composition, gas flow rate, solids flow rate, and particle size were varied. This was the first study in this area, and the results provide some new insights into the mechanism of multiparticle penetration through gas-liquid interfaces.

II. EXPERIMENTAL

The experimental apparatus is shown schematically in Figure 1. It consisted of a 230-mm diameter, 400-mm-high cylindrical "Perspex" tank, fitted with a 550-mm-long axial top-submerged 6.25-mm o.d. 5-mm i.d. brass lance. The tank was filled with water to a depth of 250 mm, with the lance tip submerged to 70 mm. A 12.5-mm o.d., 10-mm i.d. stainless steel top-submerged siphon sampling tube was located level with the lance tip, at the half-radius position. The cylindrical tank was mounted in a square-section outer Perspex tank (290 × 290 × 300 mm) filled to the same level with water to allow photography of the injected particles without optical distortion. The tank assembly was illuminated from behind with light from two 1000-W quartz lamps, diffusely reflected from a white screen to give a strong, uniform illumination of the entire vessel. The injections were recorded on video tape and photographed using a 35-mm Nikon F-801 SLR camera with a 60-mm AF Micro-Nikkor lens, at a shutter speed and aperture of 1/1000 seconds and f/16, respectively. Ilford Delta ASA 400 black and white film was used.

The solids were fed from a simple powder dispenser, which consisted of a 250-mm long, 16-mm i.d. glass container connected to the conveying line through a slide

D.E. LANGBERG, Research Fellow, and M. NILMANI, Senior Lecturer, are with G.K. Williams Cooperative Research Centre for Extractive Metallurgy, Department of Chemical Engineering, University of Melbourne, Parkville, Victoria 3052, Australia.

Manuscript submitted September 20, 1993.

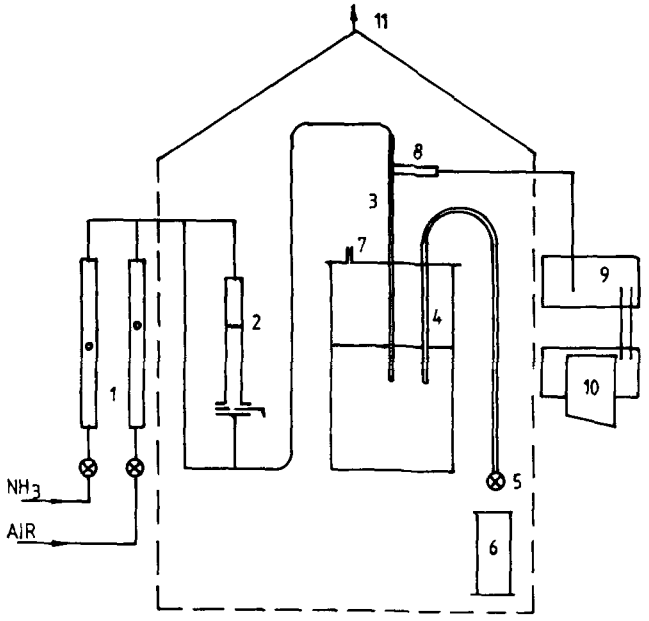

Fig. 1 — Schematic diagram of apparatus showing (1) rotameter/flow control valves; (2) powder dispenser; (3) lance; (4) siphon sampling tube; (5) on/off valve; (6) sample container; (7) vented cylindrical tank; (8) pressure transducer; (9) amplifier; (10) chart recorder; and (11) fume extraction hood.

valve. The container pressure was equalized with the pressure in the conveying line. When the slide was opened, solids flowed from the container into the conveying line at a rate governed by the size of the orifice in the slide, the particle size of the powder, and the conveying line pressure. The solids flow rate could not be set independently of the gas flow-rate with this device. The injection time was measured from a chart record of the signal produced by a pressure transducer connected to the inlet end of the lance. A charge of 10 g of powder was used for most runs. Filtered air was taken from the laboratory compressed air service through a pressure regulator, while ammonia was fed from a regulated gas bottle. The flow rates of the gases were measured and controlled through a Rotameter/needle valve assembly. The powder feeder and vessels were situated under a fume extraction hood to prevent escape of ammonia into the laboratory.

The procedure for an experiment was to set the gas flow rate at the required value, then open the slide valve to inject the powder. Immediately after completion of the powder injection, the gas flow was stopped. A 2 L sample (20 pct of bath) of liquid and solids was then withdrawn through the siphon sampling tube. The siphon was primed before the start of the run, and the suction was maintained by a ball valve at the end of the sampling line. Opening the valve enabled the sample to be withdrawn, taking approximately 22 seconds. Due to low rise velocities of solid particles in the range 0.001 to 0.002 m/s, solids concentration in the bath did not change appreciably during the sampling period. The solids were separated from the sample by filtration and weighed after drying. The concentration of the solids in the sample was calculated.

Photographs were taken during the solids injection phase of the run. The entire run was video taped for later analysis. The penetration depth of the solid particles was measured midway through the injection period from replay of the video tape and checked with photographs taken at the same time. It was found that more consistent measurements were obtained from the video tape than from short exposure-time photographs due to the fluctuating nature of the solid-liquid jet.

The settings of the controlled variables are shown in Table I. The "standard injection conditions" were defined as a gas flow rate 1.67×10^{-4} m^3 s^{-1} (10 L min^{-1}), injecting 10 g of 212- to 250-μm powder with a feeder orifice diameter of 3.4 mm. These settings produced a solids flow rate of 0.8 g s^{-1}. The size fractions of polyethylene powder were screened from a bulk sample of black polyethylene obtained from ICI Ltd. (Victoria, Australia). Anhydrous ammonia (99.99 pct NH_3) supplied by CIG Ltd. (Victoria) was used as the soluble gas. Tap water at 20 °C was used as the liquid medium. Relevant physical properties are shown in Table II.

III. EXPERIMENTAL RESULTS

A. *Particle Velocity*

A sensor was devised to measure the particle velocity at the discharge end of the lance, which consisted of two infrared emitter-detector cells mounted 50 mm apart and centered 60 mm from the end of the lance. The emitter and detector components of each cell were aligned across a hole drilled through the lance. The signal produced by particles passing the first cell was compared with the signal produced by the same particles passing the second cell on a storage oscilloscope. The time delay measured from the peak displacement between the signals was used to calculate the particle velocity. The results shown in Figure 2 indicate that the particle velocity is close to the superficial gas velocity, in contrast to other workers[16,17] who observed particle velocities substantially smaller than the conveying gas velocity. In our system, the powder dispenser was connected to the lance through 1.72 m of 6.25 mm o.d., 5 mm i.d. nylon pressure tubing, which enabled the particles to be accelerated to the gas velocity before reaching the end of the lance. The results indicate that little error is introduced by equating the exit velocity of the particles to the superficial gas velocity.

B. *Surface Tension and Contact Angle*

The surface tension of the ammonia-water interface relative to the air-water interface was measured using a variation of the "drop weight method."[18] A 2-mL pipette was fitted to a 250-mL flask in which the composition of the atmosphere could be varied. The number of drops produced when 2 mL of liquid was allowed to drip from the pipette into the flask over a 20 to 30-minute period was counted. The maximum variation in the number of drops produced under identical conditions was found to be less than 3 pct with this technique. The surface-tension ratio was related to the number of drops n and the liquid density ρ_l by

$$\frac{\sigma}{\sigma_{ref}} = \frac{\rho_l}{\rho_{ref}} \frac{n_{ref}}{n} \quad [1]$$

Table I. Injection Conditions

Gas composition (pct NH_3)	0	25	50	75	100
Gas flow rate (10^{-4} m^3 s^{-1})	0.83	1.67*	2.5	3.3	
Feeder orifice (mm)	2.7	3.4*	4.8		
Particle size (mean) (μm)	53 to 150 (101)	212 to 250* (231)			

*Standard injection conditions.

Table II. Physical Properties at 20 °C

Property	System	Value	Reference
Density	polyethylene	928 kg m^{-3}	measured
	water	1000 kg m^{-3}	14
	57.63 pct NH_4OH solution	898 kg m^{-3}	14
	ammonia gas	0.708 k gm^{-3}	14
	air	1.20 kg m^{-3}	14
Surface tension	water-air	0.07275 N m^{-1}	14
	54.37 pct NH_4OH solution (18° C)	0.05705 N m^{-1}	14
Contact angle	polyethylene-water-air	93.9 deg	15

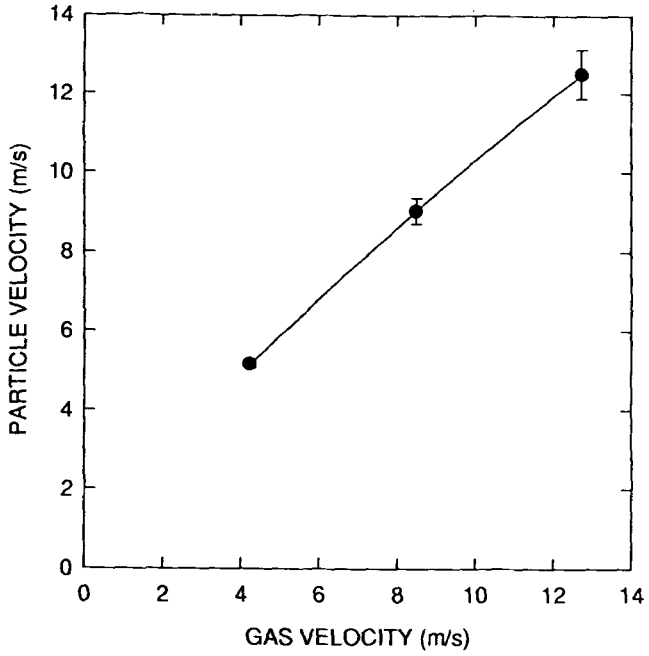

Fig. 2—Comparison of calculated gas and measured particle velocities at lance tip for 231-μm polyethylene particles injected with air (3.4-mm feeder orifice).

where σ_{ref}, n_{ref}, and ρ_{ref} refer to the air-water system. The results are shown in Table III. Experiments were carried out with a saturated ammonium hydroxide solution (28 wt pct NH_3) for comparison. The results show that the surface tension of the ammonia-water interface is identical within experimental error to that of the ammonia-ammonium hydroxide interface, which indicates that equilibrium was reached at the ammonia-water interface.

The equilibrium contact angle of the polyethylene powder in air-water and ammonia-saturated ammonium hydroxide was measured from the capillary rise through a bed of the powder.[19] The contact angle in air-water was found to be 94.5 deg, in good agreement with the accepted value for the polyethylene-air-water system of 93.9 deg. The contact angle in the ammonia-saturated ammonium hydroxide environment was found to be 89 deg. The results indicate that although the surface tension of the gas-liquid interface was considerably reduced when using ammonia, the wettability of the particles was not significantly changed.

Table III. Surface Tension of Ammonia-Water Interface

Gas-liquid	n	ρ_l	σ/σ_{ref}
Air-water	58	1000	1.0
Ammonia-water	85.5	1000	0.68
Ammonia-ammonium hydroxide	74	890	0.70

C. *Qualitative Observations of Injection Behavior*

When the polyethylene powder was injected using air, the primary bubble formed at the lance tip was elongated compared with its shape when injecting air alone.[20] The particles that accumulated around the tip of the bubble passed through the bubble surface as a "roping" discharge that disintegrated into bubble-particle aggregates in the liquid under the action of turbulence. Most of the particles did not pass through the interface individually. The bubble-particle aggregates appeared to be rafts of particles or heavily laden small gas bubbles. As they were quite bouyant, they were not projected deeply into the liquid and were rapidly entrained into the bubble plume. Photograph 1 shows the discharge of powder under the standard injection conditions using air. The formation and breakup process of the aggregates is clearly visible in this photograph.

The pumping action of the plume dominated the bulk flow patterns in the bath. The trajectory of the particles

in this flow field is shown schematically in Figure 3(a). After convection in the plume to the surface of the bath, some of the particles recirculated back into the bulk liquid, but most of them remained on the liquid surface.

When ammonia was used as the carrier gas, distinct differences were observed in the interfacial penetration behavior and trajectories of the particles. Elongation of the primary bubble occurred as with air; however, the particles appeared to penetrate into the liquid individually or as small clusters of several particles rather than bubble-particle aggregates. The ammonia bubbles rising from the lance tip dissolved rapidly once the stem linking them to the orifice severed, with few bubbles reaching the top surface of the bath.

Photograph 2 shows the discharge of the powder under standard injection conditions using ammonia. The disappearance of the plume practically eliminated the bulk circulation in the bath. The particle-liquid jet therefore pushed into an almost stagnant liquid. The jet penetration distance was increased compared to injection with air. The trajectory of the particles is shown schematically in Figure 3(b). As the particles were dispersed individually, rather than as bubble-particle aggregates, their rise velocity was lower, and they took longer to float out of the bath.

D. *Particle Dispersion*

Figure 4 shows the effect of increasing the ammonia content on the concentration of the solids dispersed in the liquid under standard injection conditions. The reported concentration is that of the liquid sample withdrawn at the half-radius position, level with the lance tip, immediately after the completion of the solids injection. The concentration was found to be approximately 10 times higher when pure ammonia was used compared with air, reflecting the increased dispersion noted in the previous section. As the liquid phase was not uniformly mixed, the measured concentration was not generally equal to the average concentration in the bulk liquid. However, the observed concentration of 0.87 g L^{-1} is close to the average bulk concentration of 1 g L^{-1}, which would result if all of the solids were retained in the liquid, indicating a high recovery of the injected powder.

Figure 5 shows the effect of increasing the gas flow rate on the solids concentration in the liquid using pure ammonia and air as the carrier gases, respectively, holding constant the average particle size (231 μm) and the feeder orifice (3.4 mm). Although the feeder orifice diameter was fixed, the solids mass flow rate was not constant but increased with increasing gas flow rate. The solids mass flow rate corresponding to each gas flow rate is listed in the caption of the figure. The solids concentration in the liquid when injecting with ammonia initially rose with increasing gas flow rate, then leveled at about 0.88 g L^{-1}, whereas it increased steadily with increasing gas flow rate for injection with air. At low gas flow rates, the ratio of the solids concentrations found for the two gases was approximately 10 but decreased to about 3 at higher gas flow rates. This convergence is to be expected, as the solids concentration for injection using ammonia at high gas flow rates is close to uniform

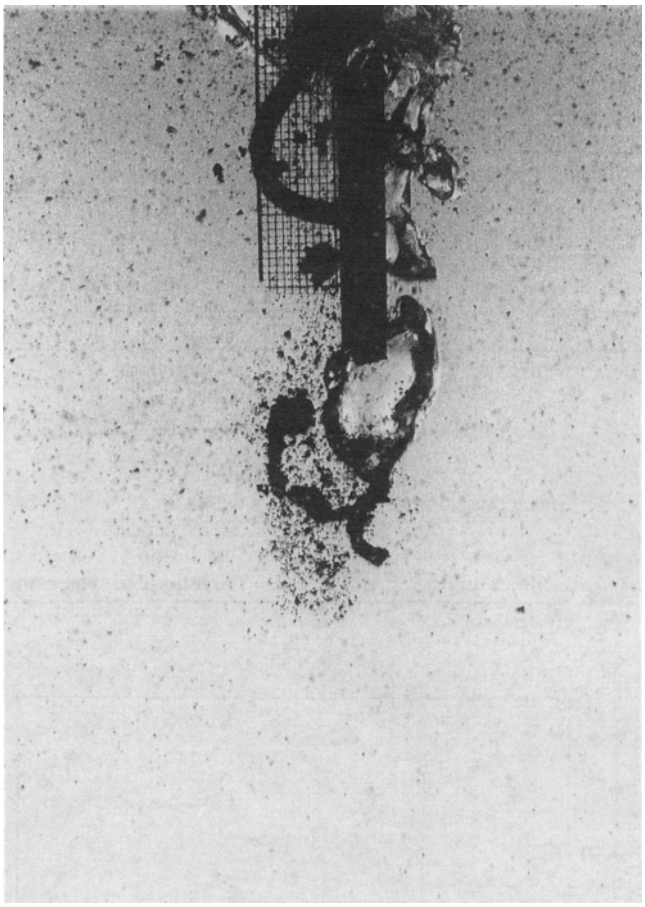

Photograph 1 — Injection of polyethylene powder using the insoluble carrier gas (Q_g = 1.67 × 10^{-4} m^3 s^{-1} air; m_s = 0.8 g s^{-1}; d_p = 231 μm). Photo shows the powder distribution at the start of injection.

dispersion and cannot rise further. In the case of injection with air, increasing the flow rate increased the injection velocity of the particles and the amount of potential energy dissipated in the bath, which contributed to deeper penetration and more effective breakup of agglomerates, respectively. These effects would have been opposed to some extent by the increased liquid entrainment into the plume carrying the particles more rapidly to the top surface of the bath.

Table IV shows the effect of the particle size on the solids concentration in the liquid for injection with air or pure ammonia at 1.67 × 10^{-4} m^3 s^{-1}, using the 3.4 mm feeder orifice. The concentration increased with increasing particle size, reflecting the lower interfacial resistance relative to inertia experienced by larger particles when penetrating through the gas-liquid interface. The extremely low concentration of 101-μm particles observed when injecting with air indicates that these particles did not penetrate through the gas-liquid interface.

E. *Jet Penetration Length*

Figure 6 shows the effect of ammonia content of the carrier gas on the total penetration length of the particle-liquid jet (distance from the lance tip to the maximum submergence of the particle-liquid jet) and the maximum

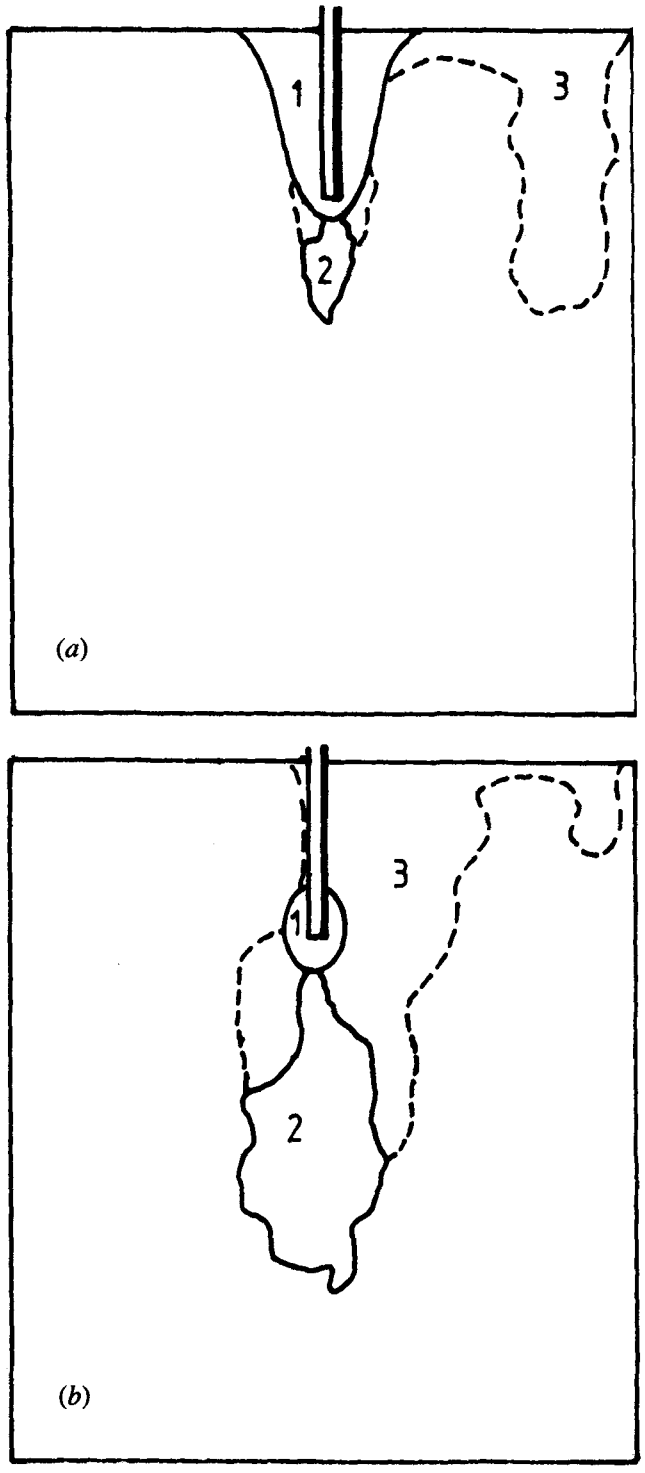

Fig. 3—Trajectories of particles injected with (*a*) insoluble carrier gas and (*b*) soluble carrier gas, showing (1) the bubble plume, (2) the particle-liquid jet, and (3) the rising particle-liquid suspension.

length of the primary bubble. Standard injection conditions were used. The total penetration length increased slowly with ammonia content up to 75 pct NH_3 and, thereafter, increased rapidly. The total penetration length using pure ammonia was found to be three times greater than with air. The bubble length decreased slightly with increasing ammonia content of the carrier gas.

Figure 7 compares the effect of increasing the solids

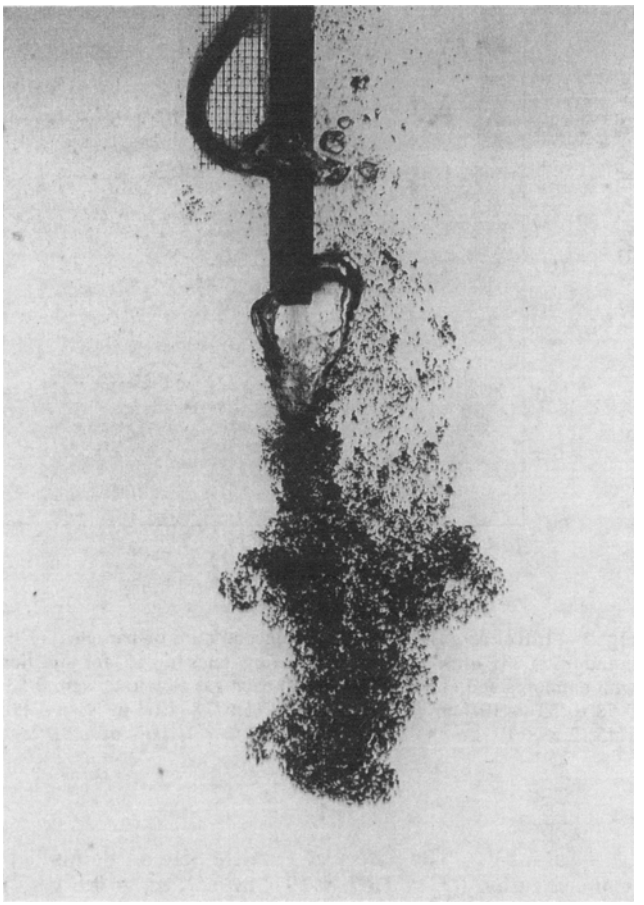

Photograph 2—Injection of polyethylene powder using the soluble carrier gas (Q_g = 1.67 × 10^{-4} m^3 s^{-1} ammonia; m_s = 0.8 g s^{-1}; d_p = 231 μm). Photo shows the powder distribution at the start of injection.

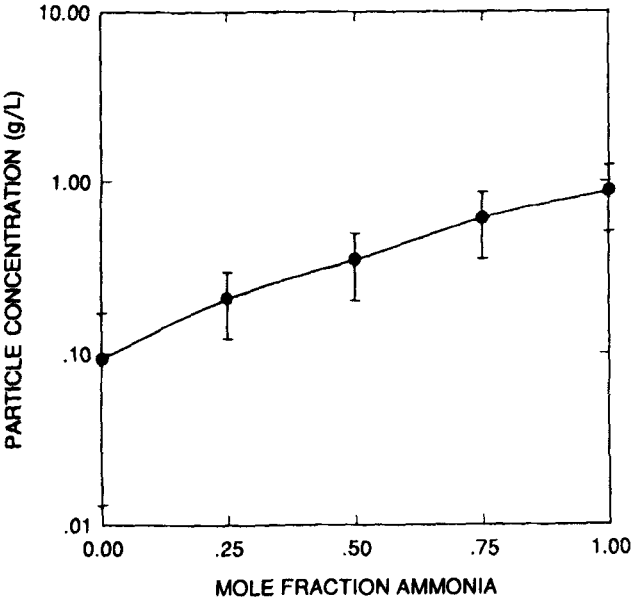

Fig. 4—Effect of carrier gas composition on concentration of particles in the liquid (Q_g = 1.67 × 10^{-4} m^3 s^{-1}; d_p = 231 μm; m_s = 0.8 g s^{-1}).

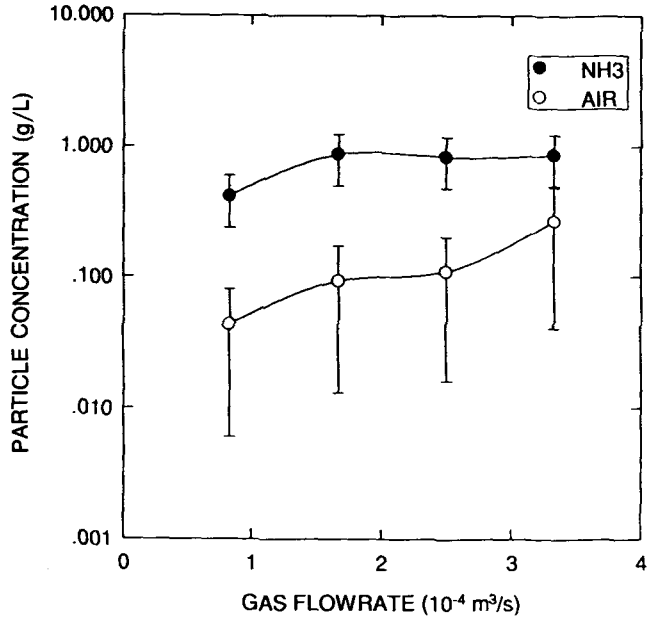

Fig. 5—Effect of gas flow rate on concentration of particles in the liquid (d_p = 231 μm). The solids mass flow rates in g s^{-1} for injection with ammonia and air, respectively, at each gas flow rate were 0.53, 0.58 (0.83 × 10^{-4} m^3 s^{-1}); 0.79, 0.80 (1.67 × 10^{-4} m^3 s^{-1}); 1.20, 1.45 (2.5 × 10^{-4} m^3 s^{-1}); and 1.22, 1.63 (3.3 × 10^{-4} m^3 s^{-1}).

Table IV. The Effect of Particle Size on Solids Concentration (Q_g = 1.67 × 10^{-4} m^3 s^{-1}; m_s = 0.8 g s^{-1})

d_p (μm)	NH_3 C (g L^{-1})	Air C (g L^{-1})
101	0.23	0.014
231	0.87	0.093

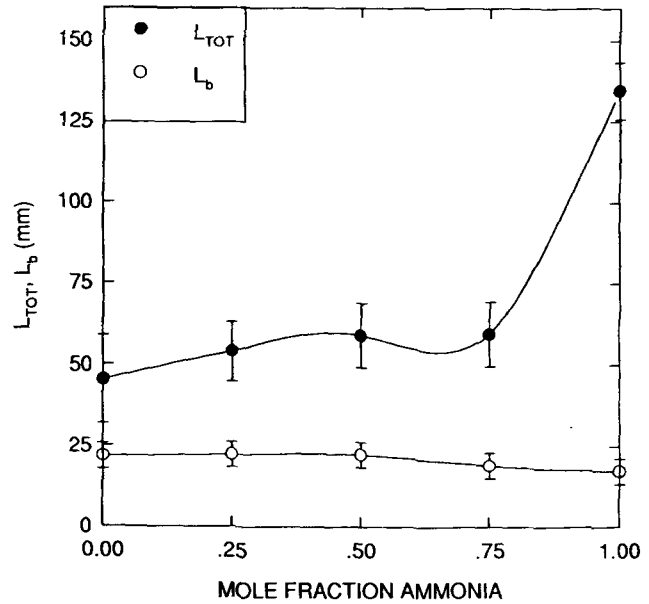

Fig. 6—Effect of carrier gas composition on the total jet penetration length L_{TOT} and the maximum bubble length L_b (Q_g = 1.67 × 10^{-4} m^3 s^{-1}; m_s = 0.8 g s^{-1}; d_p = 231 μm).

mass flow rate on the total penetration length and bubble length for injection with ammonia and air, holding the gas flow rate and particle size constant at 1.67 × 10^{-4} m^3 s^{-1} and 231 μm, respectively. The total penetration length increased with increasing solids mass flow rate for both air and ammonia. The bubble lengths also increased slightly with increasing solids mass flow rate.

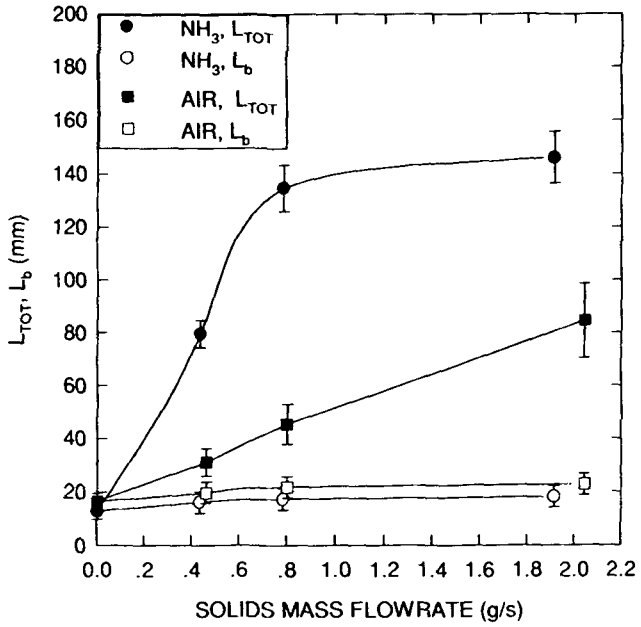

Fig. 7—Effect of solids mass flow rate on the total jet penetration length L_{TOT} and maximum bubble length L_b (Q_g = 1.67 × 10^{-4} m^3 s^{-1}; d_p = 231 μm).

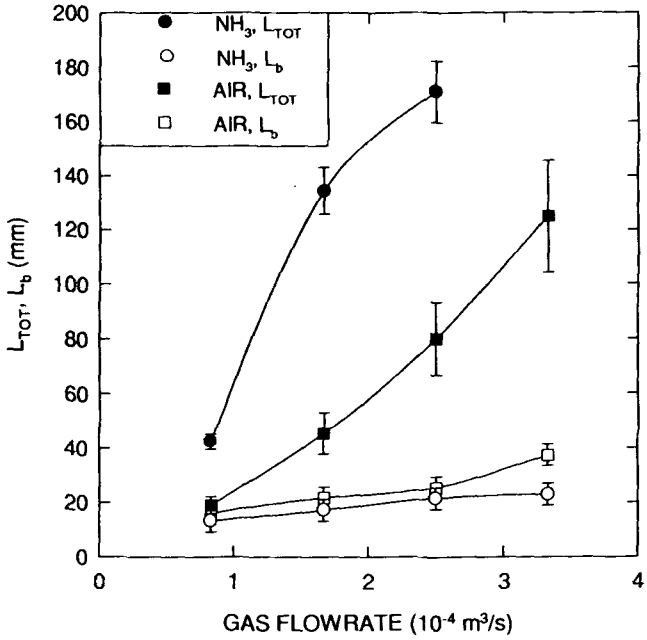

Fig. 8—Effect of gas flow rate on total jet penetration length L_{TOT} and maximum bubble length L_b (d_p = 231 μm). The solids mass flow rates in g s^{-1} for injection with ammonia and air, respectively, at each gas flow rate were 0.53, 0.58 (0.83 × 10^{-4} m^3 s^{-1}); 0.79, 0.80 (1.67 × 10^{-4} m^3 s^{-1}); 1.20, 1.45 (2.5 × 10^{-4} m^3 s^{-1}); and 1.22, 1.63 (3.3 × 10^{-4} m^3 s^{-1}).

Figure 8 compares the effect of the carrier gas flow rate on the total penetration length and bubble length, for injection of 231 μm particles with ammonia and air using the 3.4-mm feeder orifice. The penetration length and bubble length increased with increasing gas flow rate for both carrier gases. Part of the observed increase was due to the concurrent increase in the solids mass flow rate as the gas flow rate was increased.

Table V compares the effect of the average particle size on the total penetration length and bubble length, with the gas flow rate and feeder orifice fixed at 1.67×10^{-4} m^3 s^{-1} 3.4 mm, respectively. With air, a true particle-liquid jet was not formed when injecting 101 μm particles. Bubbles filled with particles detached from the primary bubble and were projected a similar distance into the liquid as the particle-liquid jet formed with 231-μm particles injected with air.

IV. DISCUSSION

The important findings of the experimental work may be summarized as follows. When the soluble carrier gas was used to inject the nonwetting powder, the dispersion of the powder in the liquid and the penetration length of the particle-liquid jet were significantly enhanced compared with injection using the insoluble carrier gas. It was also noted that the surface tension of the gas-liquid interface was decreased without a significant increase in the wettability of the powder when the soluble gas was used and that the particle exit velocity from the lance closely approximated the superficial gas velocity.

If the results for injection for the soluble and insoluble carrier gases are considered separately, it is found that they agree qualitatively with established theory. The efficiency of particle penetration through the bubble interface is reflected in the concentration of particles that were retained in the liquid after injection. For both types of carrier gas, the particle concentration increased as the gas flow rate (particle injection velocity) and the particle size were increased, as anticipated from the studies of single-particle penetration through a gas-liquid interface.[1,2,3] The penetration length of the particle-liquid jets produced by both carrier gases increased with the gas and solid flow rates, indicating a direct dependence on the momentum of the gas-solid mixture discharging from the lance, in accordance with the models of Engh *et al.*,[16] Ghosh and Lange,[17] and Farias and Irons.[6] The new information revealed by this study is the significant dependence of the degree of dispersion and penetration length on the type of carrier gas used.

The increased dispersion of the solids with the soluble carrier gas cannot be explained by changes in the surface chemistry of the solid particles, because the powder was highly nonwettable in both carrier gas systems. Instead, an explanation may be found by considering the process of particle penetration through the bubble surface. The bubble-particle aggregates observed when injecting with the insoluble gas are the result of gas entrainment by the particles as they pass through the bubble surface. In the coupled flow situations described by Irons and Tu[5] and Farias and Irons,[6] most of the carrier gas is entrained by the solids to form a gas-solid jet. The experiments carried out in this study were in the bubbling regime, where the gas was able to disengage from the solids to form the primary bubbles around the lance tip. The gas-solid mixture passing through the bubble surface, therefore, had a lower gas holdup than the mixture in the lance and possibly approached the fluidized-bed-limiting gas holdup of approximately 0.4. Once in the liquid, the gas-solid mixture was dispersed into bubble-particle aggregates held together by interstitial gas.

When the soluble gas was used, it is reasonable to suppose that the same processes took place inside the bubble. However, when the gas-solid mixture passed through the bubble surface, dissolution of the interstitial gas effectively removed the "glue" holding the bubble-particle aggregates together. The particles were released into the liquid rather than bound up inside bubble-particle aggregates.

Another important effect contributing to the higher dispersion with the soluble gas was the elimination of the bubble plume by the dissolution of the primary bubbles when they detached from the tip of the lance. Entrainment of particles into the plume zone produced by the insoluble gas resulted in their rapid convection to the upper surface of the bath, where they remained unless the recirculatory flow was sufficient to pull them back into the bulk liquid. Without the plume, the particles floated out of the liquid at a rate governed by the rise velocity due to buoyancy.

The increased concentration of particles retained by the liquid when injected with a soluble gas was a combined effect of finer dispersion immediately upon entering the liquid and a slower rate of rise out of the liquid due to reduced bulk liquid flow.

Factors contributing to the deeper penetration of the particle-liquid jet into the liquid observed with the soluble carrier gas include the lower surface tension of the gas-liquid interface, causing less dissipation of the kinetic energy of the particles striking the interface; the smaller effective size of the aggregates due to the breakup of bubble-particle aggregates by dissolution of the interstitial gas, enabling more effective coupling between the particles and the liquid; and the absence of an opposing upflow generated by the plume. Taken together with the increased dispersion, the main effect of the increased penetration depth is to increase the residence time of the particles in the liquid.

Reactive gases are currently used in a number of industrial processes including lime injection into steel using oxygen and flux injection into matte with air. In addition, all new intensive smelting reactors rely on the addition of solids such as concentrates, fluxes, and reductants to the bath while the carrier gas continues the oxidation or reduction of the molten phase.

Table V. Effect of Particle Size on Total Penetration Length and Maximum Bubble Length ($Q_g = 1.67 \times 10^{-4}$ m^3 s^{-1}; $m_s = 0.8$ g s^{-1})

	NH_3		Air	
d_p (μm)	L_{TOT} (mm)	L_b (mm)	L_{TOT} (mm)	L_b (mm)
101	92	20	57	22
231	135	17	45	16

This work is the first study in the area and has shown the potential benefits to be gained from the reactive gas-melt system for solids injection. Most common systems use air as the carrier gas, which would lead to exothermic oxidation reactions resulting in very high local temperatures, further lowering the interfacial tension and viscosity. The benefit of lower interfacial tension may assist the injection of very fine solids such as dusts.

CONCLUSIONS

A cold-model of the top-submerged injection of a non-wetting powder using soluble and insoluble carrier gases has revealed significant differences in the injection behavior of the particles and the bulk flow in the liquid bath. Conclusions were found as follows.

1. The concentration of particles dispersed in the liquid was up to 10 times higher when the soluble carrier gas was used.
2. The penetration length of the particle-liquid jet formed below the lance tip during injection was up to three times greater when the soluble carrier gas was used.
3. For both carrier gases, the concentration of dispersed particles increased with increasing gas flow rate and increasing particle size, whereas the penetration length of the jet increased with increasing gas and solids flow rates.

LIST OF SYMBOLS

C	concentration ($g \cdot L^{-1}$)
d	size (μm)
L	length (m)
m	mass flow rate ($g \cdot s^{-1}$)
n	number of drops
Q	volumetric flow rate ($m^3 \cdot s^{-1}$)
ρ	density ($kg \cdot m^{-3}$)
σ	surface tension ($N \cdot m^{-1}$)

Subscripts

b	bubble
g	gas
j	jet
l	liquid
p	particle
ref	reference liquid
s	solid
TOT	total
0	nozzle

ACKNOWLEDGMENTS

The assistance of Mr. T. Warnock with the experimental work and Ms. N. Ng with typing the manuscript is gratefully acknowledged.

REFERENCES

1. T.A. Engh, H. Sandberg, A. Hultkvist, and L.G. Norberg: *Scand. J. Metall.*, 1972, vol. 1, pp. 103-14.
2. D. Apelian, R. O'Malley, and C. Dremann: *Proc. Conf. on Scaninject II*, Lulea, Sweden, June 12–13, 1980, MEFOS, Lulea, 1980, pp. 7.1-7.33.
3. Y. Ozawa and K. Mori: *Trans. Iron Steel Inst. Jpn.*, 1983, vol. 23, pp. 769-74.
4. M. McNallan: *Proc. Conf. on Scaninject II*, Lulea, Sweden, June 12–13, 1980, MEFOS, Lulea, 1980, pp. 8.1-8.10.
5. G.A. Irons and B.-H. Tu: *Proc. Conf. on Scaninject III*, Lulea, Sweden, June 15–17, 1983, MEFOS, Lulea, 1983, pp. 11.1-11.29.
6. L.R. Farias and G.A. Irons: *Metall. Trans. B*, 1985, vol. 16B, pp. 203-09.
7. G.A. Irons and L.R. Farias: *Can. Metall. Q.*, 1986, vol. 25 (4), pp. 297-306.
8. C. Moore and R.I. Marshall: *Steelmaking*, The Institute of Metals, London, 1991, pp. 58-62.
9. M. Nilmani and D. Collins: *Proc. Conf. on Canadian Institute of Mining and Metallurgy*, Montreal, Aug. 1988, pp. 1-24.
10. B.C. Allen: in *Liquid Metals, Chemistry and Physics*, S.Z. Beer, ed., Marcel Dekker, New York, pp. 161-212.
11. F.D. Richardson: *Physical Chemistry of Melts in Metallurgy*, Academic, London 1974, pp. 426-61.
12. M. Nilmani and D.G.C. Robertson: *Trans. Inst. Min. Metall. C*, 1980, vol. 89, pp. C42-C53.
13. I.F. Taylor and J.K. Wright: *Proc. Conf. on Technological Advances in Metallurgy*, Lulea, Sweden, Sept. 20–21, 1988, MEFOS, Lulea, 1988, pp. 1-17.
14. *Handbook of Chemistry and Physics*, 57th ed., R.C. Weast, ed., CRC Press, Cleveland, OH, 1977.
15. S. Ross and I.D. Morrison: *Colloidal Systems and Interfaces*, John Wiley & Sons, New York, NY, 1988, pp. 102-03.
16. T.A. Engh, K. Larsen, and K. Venas: *Ironmaking and Steelmaking*, 1979, No. 6, pp. 268-73.
17. D.N. Ghosh and K.W. Lange: *Ironmaking and Steelmaking*, 1982, vol. 19 (3), pp. 136-41.
18. E.D. Hondros: *Techniques of Metals Research*, 1970, vol. IV, Part 2, Interscience, New York, NY, pp. 293-377.
19. R.E. Ayala, E.Z. Casassa, and G.D. Parfitt: *Powder Technol.*, 1987, vol. 51, pp. 3-14.
20. M. Nilmani, A.K. Das, A. Johnston, and T.A. Engh: *Proc. 14th Conf. on Australasian Chemical Engineering*, Adelaide, SA, Aug. 1986, Institution of Chemical Engineers, Australia, pp. 107-12.